Journal of Zhejiang University-SCIENCE A (Applied Physics & Engineering) 2022 23(12):988-997
www.jzus.zju.edu.cn; www.springer.com/journal/11582
E-mail: jzus_a@zju.edu.cn

Research Article

https://doi.org/10.1631/jzus.A2200440

Enhanced photocatalytic performance of S-doped covalent triazine framework for organic pollutant degradation

Yi SHEN[1]✉, Jing-yu HU[1], Lun LU[2], Chao ZHU[1,3]✉, Qi-le FANG[4], Shuang SONG[1]

[1]*College of Environment, Zhejiang University of Technology, Hangzhou 310032, China*
[2]*State Environmental Protection Key Laboratory of Environmental Pollution Health Risk Assessment, South China Institute of Environmental Sciences, Ministry of Ecology and Environment, Guangzhou 510655, China*
[3]*College of Chemical Engineering, Zhejiang University of Technology, Hangzhou 310032, China*
[4]*Advanced Institute of Natural Sciences, Beijing Normal University at Zhuhai, Zhuhai 519087, China*

Abstract: Photocatalysis using the abundant solar energy is an environmentally friendly and efficient way to degrade organic matter. Covalent triazine frameworks (CTFs), a new class of metal-free organic semiconductors responsive to visible light, are promising materials for water treatment. In this study, an original CTF, namely CTF-1, was modified by S-doping to form $CTFS_x$, which were used as metal-free catalysts for degradation of methyl orange (MO) and bisphenol A (BPA). The outcomes demonstrated that the photocatalytic degradation of MO and BPA by $CTFS_x$ was superior to that by CTF-1, with better stability and reusability. Within 6 h, 53.2% MO and 84.7% BPA were degraded by $CTFS_5$, and the degradation rate constants were 0.145 h^{-1} and 0.29 h^{-1}, respectively, which were 3.6 and 5.8 times higher than those of CTF-1. Further investigation revealed that enhanced visible light absorption, a reduced degree of free carrier recombination, rapid separation and transfer of photogenerated electrons and holes, and improved ·OH oxidation capacity were important factors contributing to the significantly enhanced photocatalytic activity. The S-doping method effectively improved the light absorption performance, electronic structure, and modulation band structure of CTF-1. This work highlights the potential application of low-cost metal-free catalysts driven by visible light for the removal of organic pollutants from wastewater.

Key words: Covalent triazine frameworks (CTFs); Photocatalysis; S-doping; Organic pollutant removal

1 Introduction

With rapid industrialization, various organic compounds have contributed to the deterioration of water quality, posing a huge threat to ecosystems and human health (Boelee et al., 2019). Hence, the control of wastewater contamination has become vital. In particular, the treatment of organic pollutants in wastewater has turned into a research hotspot conducive to the improvement of water ecosystem quality (Hu et al., 2022). Millions of organic compounds have been synthesized, especially pharmaceuticals, dyes, personal care products, pesticides, and commonly used organic compounds (Lu and Astruc, 2020). Methyl orange (MO) and bisphenol A (BPA) are typical organic pollutants which have a non-negligible impact on the environment and health (Xu et al., 2023). A new advanced oxidation technology, photocatalytic technology, is an effective means to treat organic pollutants in water, since it is able to mineralize organic pollutants into the non-toxic inorganic substances CO_2 and H_2O, and does not produce secondary pollution.

Covalent triazine frameworks (CTFs) are special covalent organic frameworks (COFs) generated through the cyano-trimerization of aromatic cyanide compounds. They are free of metal elements, and have high chemical stability, a rich nitrogen content, and visible light absorption ability, making them well suited for applications in the fields of hydrogen production and photocatalytic degradation (Huang et al., 2019; Qian et al., 2021; Sarkar et al., 2021). However,

✉ Yi SHEN, shenyi@zjut.edu.cn
Chao ZHU, zhuchao@zjut.edu.cn
Yi SHEN, https://orcid.org/0000-0001-8977-7569
Chao ZHU, https://orcid.org/0000-0002-0971-7951

Received Sept. 12, 2022; Revision accepted Oct. 14, 2022; Crosschecked Dec. 1, 2022

the photocatalytic efficiency of the original CTFs was generally limited by their shortcomings of insufficient visible light absorption and low charge mobility (Huang et al., 2018; Shen et al., 2019; Hu et al., 2020). Recently, metal doping has become a promising technology in the field of heterogeneous catalytic processes. For example, it has been reported that doped Fe^{3+} CTF could speed up charge separation and conversion by serving as a photocatalytic active center and "electron relay" (Gao et al., 2021), which significantly improved the photocatalytic performance of original CTF (CTF-1). Moreover, a novel Na-doped covalent triazine-based framework (H-CTF-Na) was designed in which Na-doping narrowed the band gap, while 3D layered nanocellular morphology improved light harvesting and electronic transfer (Zhu et al., 2021b). The above studies showed that metal doping could optimize the performance of CTFs, but the technology could not be popularized due to the disadvantages of metal dissolution and high cost. Therefore, doping non-metallic elements into photocatalysts has been gradually considered as a feasible strategy to improve photocatalytic performance due to its special advantages in creating more active sites and accelerating the separation and transport of charge carriers (Niu et al., 2021). In recent years, the photocatalytic properties of CTFs have been optimized by doping of elements including silicon, phosphorus, and elemental nitrogen, thereby modifying the morphology and electronic structure of CTF catalysts. This also enhanced their photocatalytic performance to a certain extent (Cheng et al., 2018; Cao et al., 2019; Ball et al., 2020). The most commonly used dopant was elemental sulfur (S), which can regulate the electronic structure and optical absorption characteristics of carbon-based organic semiconductor photocatalysts (Li JH et al., 2012; Wang et al., 2014; Li LY et al., 2016). However, the doping effect of S into CTF in photocatalytic degradation of pollutants has not been studied. In particular, the effects on energy band structure and electronic structure are not clear.

In this study, original CTF-1 and modified CTF-1 doped with three different S contents ($CTFS_x$) were synthesized by high temperature annealing. The $CTFS_x$ showed effective charge transfer and wide visible light absorption, and were used as photocatalysts for the degradation of MO and BPA. The kinetics and reusability of $CTFS_x$ in the degradation of organic pollutants were evaluated, and a mechanism of action is proposed based on a free radical trapping experiment. The results indicate a practical and effective method for removing organic pollutants from water, and provide a feasible method for designing and optimizing CTF-based photocatalysts.

2 Experimental methods

2.1 Synthesis of original CTF-1 and S-doped CTF-1

To synthesize CTF-1, a blend of 1,4-dicyanobenzene B (DCB, 4 mmol) and trifluoromethanesulfonic acid (CF_3SO_3H, 2.5 mL) was stirred in an ice bath at 0 °C to form a viscous yellow gel. It was then transferred to an oven and heated at 100 °C for 20 min to form a yellow solid. Then, the white powder, called CTF-1, was obtained by washing with alcohol water. To obtain S-doped CTF ($CTFS_x$), element S (with the mass of 0.004 g, 0.008 g, and 0.02 g) and CTF-1 (0.4 g) were mixed uniformly in an agate mortar, and then the mixed material was placed in a tube and annealed in a furnace at 250 °C for 1 h. The heating rate was 5 °C/min, and the flow rate of Ar gas (purity> 99.999%) was 0.1 L/min. After cooling to room temperature, it was thoroughly ground by the agate grinding method. Then the $CTFS_x$ (x=1, 2, 5) were synthesized by refluxing in ethanol solution at 170 °C for 32 h.

2.2 Catalyst characterization

The morphology of the samples was investigated using scanning electron microscopy (SEM), high-resolution transmission electron microscopy (HRTEM), and Brunauer-Emmett-Teller (BET) specific surface area. SEM was performed on a Nova Nano SEM 450 (FEI, USA), and HRTEM by Tecnai G2F30 S-Twin TEM (FEI, USA). BET surface area estimation using nitrogen adsorption-desorption was performed at −196 °C on a NOVA-2000E surface area analyzer. The chemical structures of CTF-1 and $CTFS_x$ were analyzed by Fourier transform infrared spectroscopy (FT-IR), which was recorded in the wavenumber range of 4000–500 cm^{-1} with a resolution of 4 cm^{-1}, using a Nicolai Thermo NEXUS 670 spectrometer. Photoelectrochemical performance was examined by ultraviolet-visible diffuse reflectance spectroscopy

(UV-Vis DRS), electrochemical impedance spectroscopy (EIS), and photocurrent responses. All UV-Vis DRS studies of CTFs were performed using a Shimadzu UV-2550, with $BaSO_4$ as a UV-Vis spectrophotometer in the wavelength range of 200–800 nm baseline correction reference.

2.3 Evaluation of photocatalytic performance of CTFs

The experiment was carried out in a cylindrical quartz photoreactor with a double water jacket (outer diameter 80 mm, inner diameter 55 mm, and height 100 mm). The reaction temperature was controlled by circulating water at 25 ℃. A 400-W xenon lamp was placed vertically in the quartz cooling water jacket. Each 20-mg sample was suspended and dispersed in 80-mL and 1-mg/L MO solution, and the adsorption equilibrium was achieved by stirring in the dark for 0.5 h. During the reaction process, samples were taken with a 1-mL syringe and filtered through a 0.22-μm filter element during the specified time period (0–6 h). The resulting solution was analyzed at 463 nm using a UV1800PC spectrophotometer (USA). The photocatalytic degradation process of BPA is similar to that of MO, and the concentration of BPA was analyzed by an Agilent 1260 HPLC equipped with a fluorescence detector. The flow phase and the detection wavelength were set as methanol/water (70:30 in volume), λ=225 nm of BPA. Corresponding traps were added for the free radical capture experiment: disodium ethylenediaminetetraacetate (EDTA-2Na: 100 mmol/L), p-benzoquinone (p-BQ: 2 mmol/L), and isopropanol (IPA: 100 mmol/L) were selected as the traps of holes (h^+), superoxide radicals ($\cdot O_2^-$), and hydroxyl radicals ($\cdot$OH), respectively.

2.4 Cycle experiment

The residual CTFs of the cyclic reaction were filtered and collected, and the residual pollutants on the sample surface were washed by deionization. The washed powders were then freeze-dried. For the next cyclic reaction, the recycled CTFs with negligible mass loss were added to an aqueous solution containing organic contaminants (BPA). Next, the suspension was stirred in the dark until well combined. After the balance of adsorption and desorption was achieved, the next cyclic photocatalytic experiment was carried out according to other cyclic reaction conditions.

3 Results and discussion

3.1 Characterisation of pristine CTF-1 and $CTFS_x$

The morphology of the synthesized samples was analyzed by SEM and HRTEM. Fig. 1 shows that the original CTF-1 exhibited a smooth and dense nanosheet structure, consistent with previous reports (Cheng et al., 2018). When different contents of S element were introduced into CTF-1, $CTFS_x$ retained the nanolamellar structure, but showed partial compaction, breakage, and wrinkling (Li et al., 2016). This may have been because the structure of CTF-1 was destroyed by high-temperature calcination to a certain extent. The degree of compaction and fragmentation

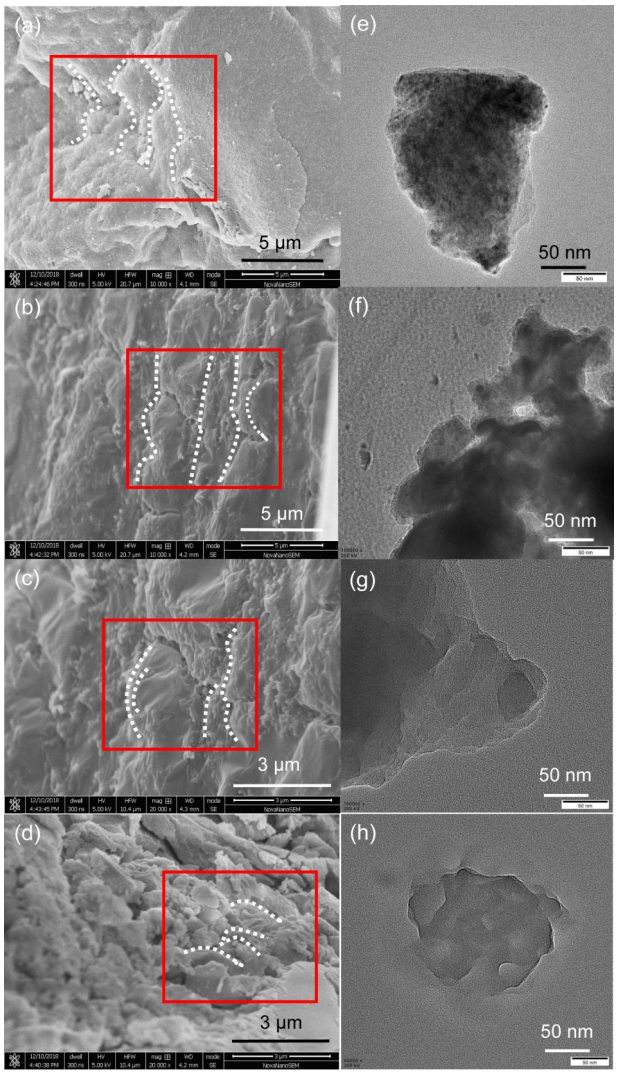

Fig. 1 SEM images of CTF-1 (a), $CTFS_1$ (b), $CTFS_2$ (c), and $CTFS_5$ (d), and TEM images of CTF-1 (e), $CTFS_1$ (f), $CTFS_2$ (g), and $CTFS_5$ (h)

was exacerbated by increasing S content. These nanosheets might contribute to electron migration on the layer, promoting the transfer of photogenerated charge carriers along the nanosphere under visible light conditions, retarding the compounding of holes with electrons and thereby facilitating photocatalysis (Ge et al., 2020).

The BET surface area and corresponding pore volume of the CTFs are summarized in Table S1 of the electronic supplementary materials (ESM). According to the BET average pore size distribution calculation, the pore sizes of CTF-1, $CTFS_1$, $CTFS_2$, and $CTFS_5$ were 5.63, 6.78, 7.20, and 8.55 nm, respectively, indicating that the material was full of mesopores and the pore size increased after S-doping. This was more conducive to the diffusion of pollutants because they could enter the interior of CTFs through these pores and be adsorbed inside (Kong et al., 2022; Xu et al., 2022). The specific surface zones of the four materials were 23.43 m^2/g (CTF-1), 35.67 m^2/g ($CTFS_1$), 37.88 m^2/g ($CTFS_2$), and 42.51 m^2/g ($CTFS_5$), respectively, which meant the doping of S increased the specific surface area of the CTF. This might be conducive to the capture of visible light (Zhang et al., 2019). Thus, $CTFS_x$ may contribute to pollutant removal in terms of providing more active sites and increasing the utility of visible light.

The conjugated skeleton structure was maintained after S-doping, which coincided with the FT-IR (Fig. 2a) results (Li et al., 2016). The peaks at 1510 cm^{-1} and 1352 cm^{-1} for all CTFs were attributed to C=N and C–N on newly formed triazine rings (Ren et al., 2012; Zhu et al., 2022). However, due to the low S content, there was no peak reflecting combination with other elements. The peaks in the range of 1200–1610 cm^{-1} could be attributed to the C–N, C=N heterocyclic stretching vibrational mode, and decreased with increasing S-doping. This suggested that the introduced S could potentially replace the N atom on the triazine ring (Feng et al., 2021). When S was doped by calcination, the triazine ring was more easily damaged than the benzene ring. Also, high temperatures break C–N and C=N bonds, resulting in S replacing the N to form C–S and C=S bonds with the addition of one electron (Zhu et al., 2018).

To investigate whether S-doping changed the band structure of the material, UV-Vis diffuse reflectance spectra were measured. UV-Vis DRS analysis

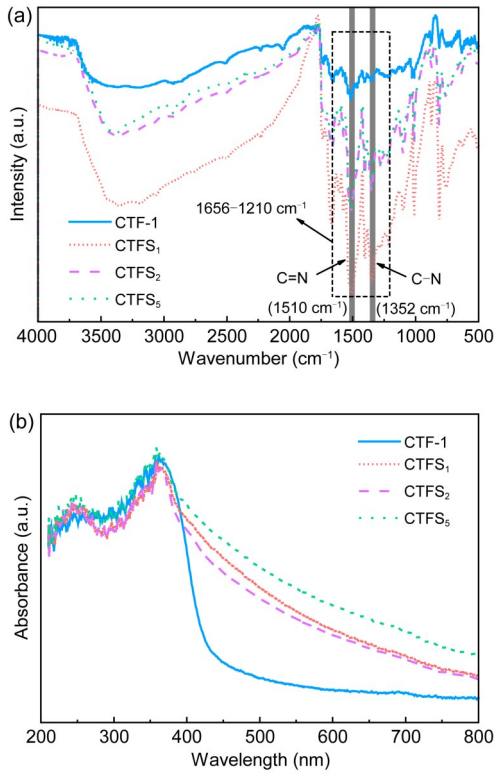

Fig. 2 FT-IR spectra (a) and UV-Vis DRS spectra (b) of CTF-1 and $CTFS_x$

(Fig. 2b) reflected the light absorption properties of the material. CTF-1 showed a semiconductor-like absorption at 441 nm, and the absorption region of $CTFS_x$ extended into the visible region. Meanwhile, the optical absorption intensity became stronger in almost the entire wavelength range with increasing S-doping. This indicated that the S-doping effect widened the electron delocalization range of the CTF network. The band gap of the $CTFS_x$ sample gradually narrowed from 2.90 to 2.78 eV (Fig. S1 of the ESM), and the valence band (VB) increased from 2.46 to 2.50 eV accordingly (Fig. S2 of the ESM). Meanwhile, the conduction band (CB) moved from −0.54 to −0.28 eV. The slow broadening of VB and progressive reduction of CB shortened the electron transfer path between VB and CB, facilitating electron excitation and rapid transfer to the material surface (Zhu et al., 2023). The results indicate that S element doping further tuned the band structure and redox properties of CTF-1.

EIS and photocurrent responses were used to investigate the charge separation efficiency of CTFs. The arc radii of the electrochemical impedance spectra of

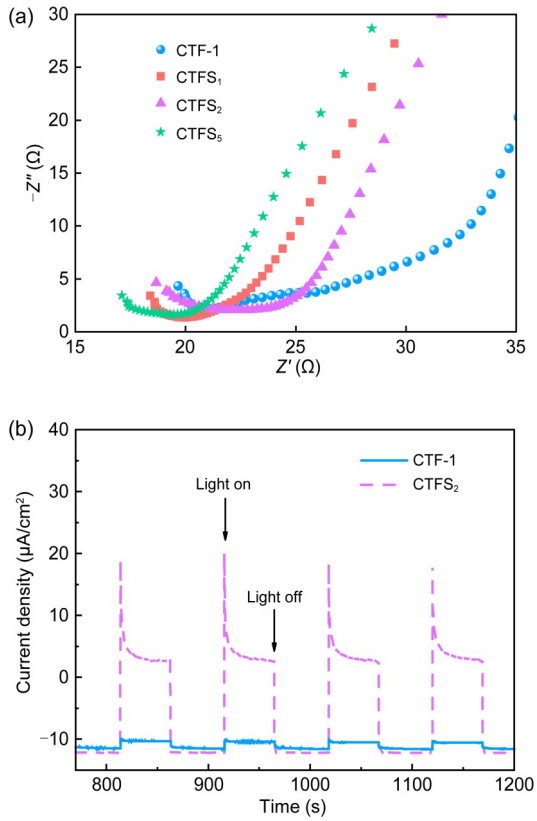

Fig. 3 EIS diagram of CTF-1 and $CTFS_x$ (a) and photocurrent time response curves (b). *Z′* is the impedance, and *Z″* is the capacitive resistance

$CTFS_x$ samples were all smaller than those of CTF-1 (Fig. 3a), and the decreasing trend was consistent with the increasing trend of photoactivation activity. This indicates that the S element promoted the migration of photogenerated charge during the photocatalytic process, so that more charge carriers transferred to the surface active sites participating in the reaction before recombination, which contributed to the improvement of the photocatalytic performance (Hong et al., 2021; Zhu et al., 2021a). The Mott-Schottky (M-S) plot (Fig. S3 of the ESM) shows that the flat-band potential estimates of CTF-1, $CTFS_1$, $CTFS_2$, and $CTFS_5$ were −0.54, −0.50, −0.39, and −0.28 eV, respectively. In addition, the photocurrent time-response curves of pristine CTF-1 and $CTFS_2$ (Fig. 3b) showed that the photocurrent intensity of $CTFS_2$ was significantly enhanced relative to CTF-1, indicating that the photogenerated charge carriers were more efficiently separated. This was because the sample nanosheet structure promoted the rate of electron transfer across layers (Ventosa et al., 2013).

3.2 Photocatalytic degradation of MO and BPA by CTFs

MO and BPA, as representative contaminants of dyes and pharmaceutical and personal care products (PPCPs), were used as probes to detect the photocatalytic ability of the materials and effects of hydroxyl functional groups in pollutant molecules.

The photocatalytic degradation of MO by four kinds of CTFs was evaluated after adsorption equilibrium. Under visible light irradiation, with increasing S-doping content, the order of degradation rate of photocatalytic degradation of MO from high to low was $CTFS_5$>CTF-1>$CTFS_1$>$CTFS_2$ (Fig. 4a). The degradation efficiency of $CTFS_5$ on MO reached 53.23% within 6 h, indicating that $CTFS_5$ had the best photocatalytic effect among the four catalysts, while $CTFS_1$ and $CTFS_2$ showed weaker photocatalytic performance than CTF-1. This may have been because the content of contaminants entering the pores was affected by doping that changed the morphology of the sample.

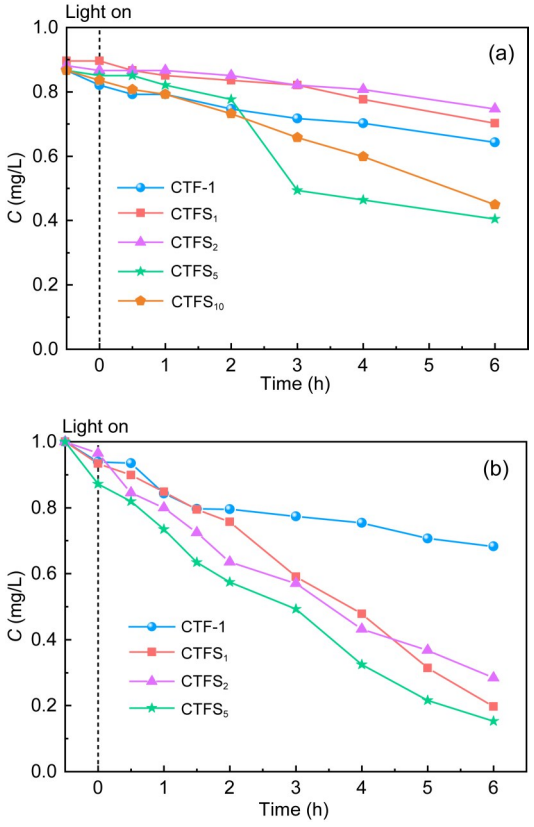

Fig. 4 Removal efficiencies *C* of MO (a) and BPA (b) by CTFs before and after visible light irradiation

To investigate whether CTF-1 and $CTFS_x$ had similar photocatalytic degradation ability for different organic pollutants, another organic pollutant, BPA, was selected for testing under the same experimental conditions. BPA is a toxic organic chemical widely used in industry. Clearly, the data line trend of BPA degradation in Fig. 4b was similar to that of MO. As the irradiation time increased, the concentration of BPA decreased continuously. After 4-h irradiation, the order of removal efficiency of pollutants was $CTFS_5$>$CTFS_2$>$CTFS_1$>CTF-1, which indicated that the photocatalytic degradation of BPA solution by the $CTFS_x$ catalysts was stronger than that by CTF-1. After 6-h visible light irradiation, the degradation effect of CTF-1 on BPA tended to be gentle, and the degradation efficiency was 31.7%. In contrast, the photocatalytic degradation of BPA was significantly improved by $CTFS_x$. The degradation efficiency of BPA by $CTFS_5$ was as high as 84.7%, which may be attributed to the enhanced oxidative capacity of $CTFS_x$. Moreover, as the active site, S had a large electronegativity and was an electron withdrawing group, while the hydroxyl group in the BPA molecule was an electron donating group, facilitating contact between them (Hu et al., 2011; He et al., 2021).

To better analyze the kinetic differences among CTFs in photocatalytic degradation, first-order kinetic fitting was adopted for the degradation processes of the two pollutants. The results are shown in Fig. 5. $CTFS_5$ maintained the highest degradation rates of MO (0.145 h^{-1}) and BPA (0.29 h^{-1}). They were 3.6 times and 5.8 times higher than those of CTF-1, which were comparable to photocatalytic activity.

After 6-h irradiation, the efficiencies of photocatalytic degradation of MO and BPA both followed the order $CTFS_5$>$CTFS_{10}$>$CTFS_2$>$CTFS_1$>CTF-1 (Fig. S4 of the ESM). The pollutant removal ratios of $CTFS_{10}$ were 48.2% for MO and 81.2% for BPA, which were significantly lower than those of $CTFS_5$ (53.2% for MO and 84.7% for BPA). This indicates that further S-doping did not improve the photocatalytic performance of $CTFS_x$, which also confirmed the high photocatalytic activity of $CTFS_5$.

3.3 Recycling experiment

A cyclic test was used to evaluate the stability and recyclability of $CTFS_5$ for BPA photodegradation. The results showed that the photocatalytic degradation rate was 77.1% at the end of the first cycle test (Fig. 6). After four cycles of testing, the BPA degradation efficiency was only partially reduced, indicating that $CTFS_5$ had excellent stability and reusability in the photocatalytic degradation of organic matter. This provides a strong experimental basis for the promotion and application of $CTFS_x$ to remove organic pollutants in water bodies.

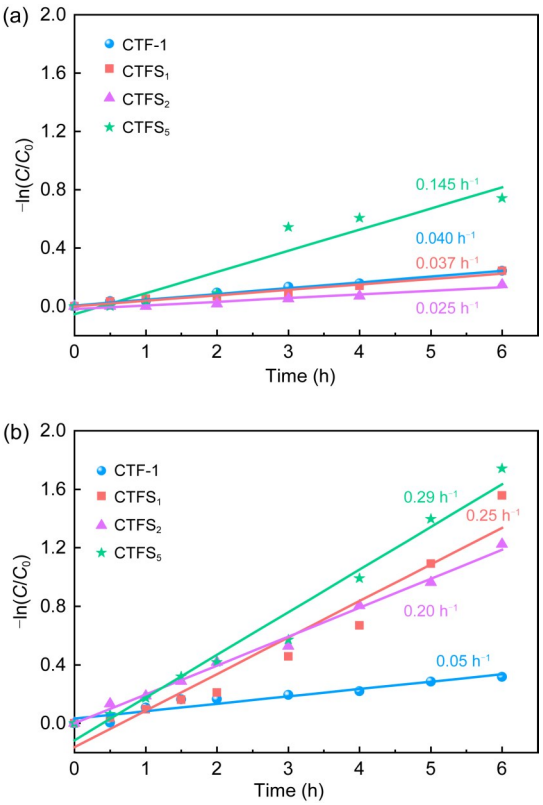

Fig. 5 First-order kinetic fitting of CTF-1 and $CTFS_x$ on photocatalytic degradation of MO (a) and BPA (b). C_0 is the initial concentration when the light time is 0

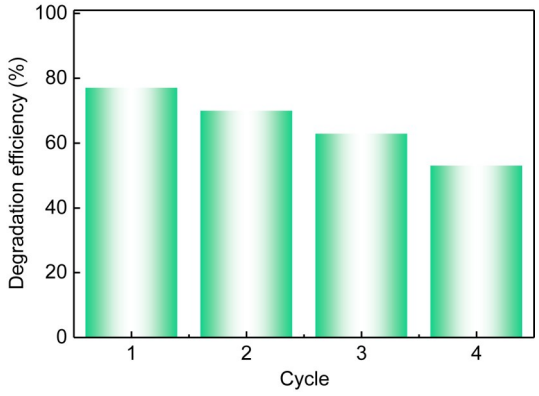

Fig. 6 Cycling experiments of $CTFS_5$ degradation of BPA

3.4 Degradation mechanism of MO and BPA by CTFs

The degradation mechanism could be described in terms of two factors: the reactive oxygen species (ROS) and material properties.

In the process of photocatalytic degradation of MO and BPA, ROS such as hydroxyl groups (·OH), superoxide radicals ($\cdot O_2^-$), and holes (h^+) may play a key role (Vickers, 2017). To identify the main active species involved in the photocatalytic process, radical trapping experiments were performed. The degradation of BPA by $CTFS_5$ was selected as a control experiment. p-BQ, EDTA-2Na, and IPA were added to BPA to capture $\cdot O_2^-$, h^+, and ·OH, respectively. The addition of EDTA-2Na and p-BQ did not significantly inhibit the photocatalytic degradation of photogenerated h^+ and $\cdot O_2^-$ (Fig. 7). However, the removal rate of BPA decreased by 75.5% after adding IPA to BPA, indicating that ·OH was the main ROS in this reaction and could actively promote the photodegradation of BPA. Under visible light irradiation, $CTFS_5$ could be excited to generate electrons as well as holes, migrate to the surface of the photocatalyst, and evolve further to generate active species. The possible pathways for the photodegradation of organic pollutants by $CTFS_x$ were explained by the following reactions:

$$CTFS_x + hv \rightarrow CTFS_x(h^+) + CTFS_x(e^-), \quad (1)$$

$$CTFS_x(h^+) + H_2O \rightarrow OH + H^+, \quad (2)$$

$$OH + MO/BPA \rightarrow products\,(CO_2 + H_2O). \quad (3)$$

Because the CB of $CTFS_5$ (−0.28 V) was more correct than that of $O_2/\cdot O_2^-$ (−0.33 V), theoretically the

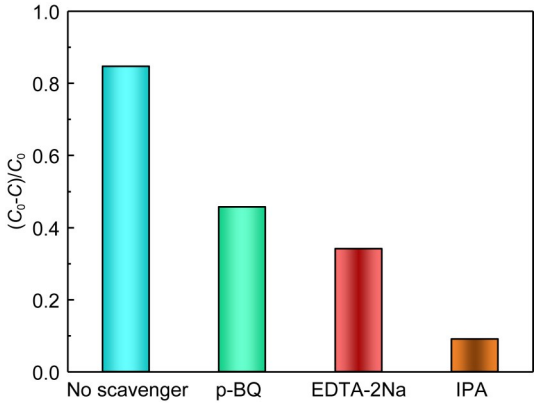

Fig. 7 Performance of $CTFS_5$ with different radical scavengers for photodegradation of BPA under the same reaction conditions

electrons accumulated on the CB of CTF cannot be captured by adsorbed oxygen to generate $\cdot O_2^-$. $\cdot O_2^-$ is almost absent from photocatalytic systems (Zhu et al., 2020). However, the positive VB of $CTFS_5$ (+2.50 V) was higher than that of CTF-1 (+2.46 V), indicating that the oxidation capacity of $CTFS_5$ was enhanced. Thus, h^+ can directly oxidize water molecules to generate ·OH, providing a continuous stream of active species for pollutant degradation. This was one of the factors of $CTFS_5$ that enhanced the photocatalytic degradation of MO and BPA.

There were three main reasons why S-doping improved the photocatalytic performance of CTF-1 in removing organic pollutants from water. The possible photocatalytic mechanism is shown in Fig. 8. Firstly, the nanosheet morphology facilitated the transfer of electrons in the layer, and the S-doping caused the originally uniform molecular dipole moment of the CTF to be broken. This resulted in an electron transfer path

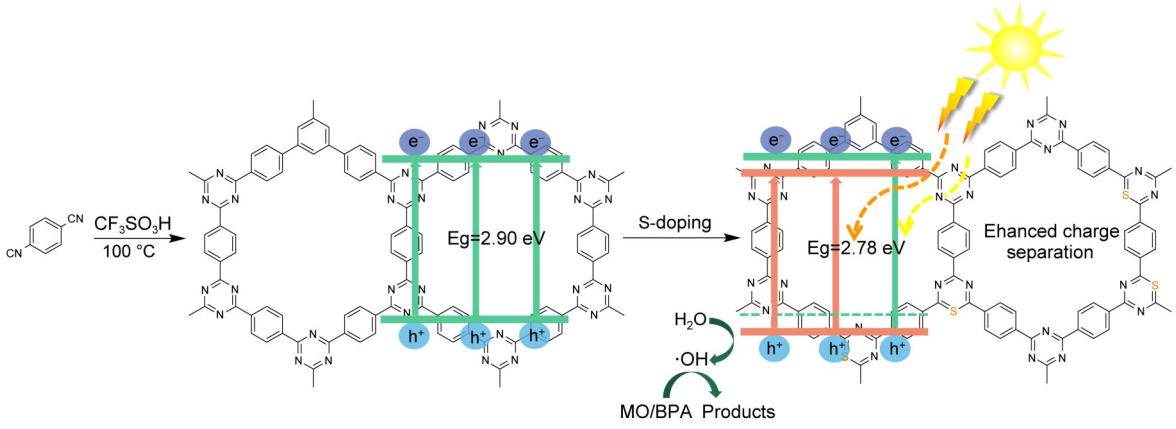

Fig. 8 Removal mechanism diagram of MO/BPA by $CTFS_x$. Eg represents the band gap

from high potential energy to low acoustic potential energy, delaying the recombination of photogenerated electrons and holes. Secondly, the narrowed band gaps of S-doped CTFs shifted the absorption band edge to the visible light region, where more visible light photons could be captured and more carriers photogenerated. Thirdly, the doping of S decreased the VB energy of $CTFS_x$, thereby increasing their pollutant oxidation ability. The narrowed band gap and reduced VB site had a synergistic effect, improving light absorption and enhancing the oxidation ability of photogenerated holes. The above features enabled $CTFS_x$ to generate ·OH ROS, which played a critical part in the removal of organic pollutants. These results demonstrated that doping S in CTF-1 could enhance the absorption of visible light and reduce the degree of free carrier recombination. This promoted the rapid separation and transfer of photogenerated electrons and holes, further enhancing the oxidative ability of ·OH, and finally improving the photocatalytic efficiency.

4 Conclusions

The element S was introduced into the triazine ring of CTF-1 and a series of $CTFS_x$ doped with different contents of S were successfully prepared. Compared with the original CTF-1, the S-doped CTF showed excellent photocatalytic activity and cyclic stability. $CTFS_5$ exhibited the best photocatalytic performance. Within 6 h of visible light catalytic reaction, 53.2% MO and 84.7% BPA were degraded, and the degradation rate constants reached 0.145 h^{-1} and 0.29 h^{-1}, respectively, which were 3.6 times and 5.8 times higher than that of CTF-1. A mechanism of photocatalytic degradation of MO and BPA by $CTFS_x$ was also proposed. We demonstrated that the active oxidizing species ·OH was mainly involved in the degradation of organic pollutants to carbon dioxide and water. We proved that the enhanced visible light absorption, narrowed band gap, corrected VB position, and faster photogenerated charge transfer were the main reasons for the markedly improved photocatalytic activity of $CTFS_5$. This work shed light on the design of metal-free catalysts with enhanced visible light harvesting and charge separation, showing the potential for practical applications in sunlight-driven removal of organic pollutants from wastewater.

Acknowledgments

This work is supported by the National Natural Science Foundation of China (Nos. 22006131 and 22276171), the Zhejiang Provincial Natural Science Foundation of China (No. LQ20B070010), the China Postdoctoral Science Foundation (Nos. 2020T130598 and 2019M662106), and the Fund of Zhuhai Science and Technology Bureau, China (No. ZH22017003210025PWC).

Author contributions

Yi SHEN designed the research. Jing-yu HU and Chao ZHU performed the tests and processed the corresponding data. Jing-yu HU wrote the first draft of the manuscript. Lun LU, Qi-le FANG, and Shuang SONG helped to organize the manuscript. Yi SHEN and Chao ZHU revised and edited the final version.

Conflict of interest

Yi SHEN, Jing-yu HU, Lun LU, Chao ZHU, Qi-le FANG, and Shuang SONG declare that they have no conflict of interest.

References

Ball B, Chakravarty C, Sarkar P, 2020. Silicon and phosphorus Co-doped bipyridine-linked covalent triazine framework as a promising metal-free catalyst for hydrogen evolution reaction: a theoretical investigation. *The Journal of Physical Chemistry Letters*, 11(4):1542-1549. https://doi.org/10.1021/acs.jpclett.9b03876

Boelee E, Geerling G, van der Zaan B, et al., 2019. Water and health: from environmental pressures to integrated responses. *Acta Tropica*, 193:217-226. https://doi.org/10.1016/j.actatropica.2019.03.011

Cao YQ, Zhu YZ, Chen XF, et al., 2019. N-doped hierarchical porous metal-free catalysts derived from covalent triazine frameworks for the efficient oxygen reduction reaction. *Catalysis Science & Technology*, 9(23):6606-6612. https://doi.org/10.1039/C9CY01597C

Cheng Z, Fang W, Zhao TS, et al., 2018. Efficient visible-light-driven photocatalytic hydrogen evolution on phosphorus-doped covalent triazine-based frameworks. *ACS Applied Materials & Interfaces*, 10(48):41415-41421. https://doi.org/10.1021/acsami.8b16013

Feng CY, Tang L, Deng YC, et al., 2021. A novel sulfur-assisted annealing method of g-C_3N_4 nanosheet compensates for the loss of light absorption with further promoted charge transfer for photocatalytic production of H_2 and H_2O_2. *Applied Catalysis B: Environmental*, 281:119539. https://doi.org/10.1016/j.apcatb.2020.119539

Gao SJ, Zhang P, Huang GC, et al., 2021. Band gap tuning of covalent triazine-based frameworks through iron doping for visible-light-driven photocatalytic hydrogen evolution. *Chemsuschem*, 14(18):3850-3857. https://doi.org/10.1002/cssc.202101308

Ge WY, Jiao SY, Xu MM, et al., 2020. Trioctylphosphine

(TOP)-free synthesis of $TiSe_2$ plates for enhanced photocatalytic degradation performance of Rhodamine B dyes. *Solid State Sciences*, 103:106189. https://doi.org/10.1016/j.solidstatesciences.2020.106189

He SX, Yin RL, Lai TY, et al., 2021. Structure-dependent degradation of nitroimidazoles by cobalt-manganese layered double hydroxide catalyzed peroxymonosulfate process. *Chemosphere*, 266:129006. https://doi.org/10.1016/j.chemosphere.2020.129006

Hong Y, Cho Y, Go EM, et al., 2021. Unassisted photocatalytic H_2O_2 production under visible light by fluorinated polymer-TiO_2 heterojunction. *Chemical Engineering Journal*, 418:129346. https://doi.org/10.1016/j.cej.2021.129346

Hu SY, Sun YN, Feng ZW, et al., 2022. Design and construction strategies to improve covalent organic frameworks photocatalyst's performance for degradation of organic pollutants. *Chemosphere*, 286:131646. https://doi.org/10.1016/j.chemosphere.2021.131646

Hu YB, Gao XK, Di CA, et al., 2011. Core-expanded naphthalene diimides fused with sulfur heterocycles and end-capped with electron-withdrawing groups for air-stable solution-processed n-channel organic thin film transistors. *Chemistry of Materials*, 23(5):1204-1215. https://doi.org/10.1021/cm102850j

Hu YP, Huang W, Wang HS, et al., 2020. Metal-free photocatalytic hydrogenation using covalent triazine polymers. *Angewandte Chemie International Edition*, 59(34):14378-14382. https://doi.org/10.1002/anie.202006618

Huang W, Byun J, Rörich I, et al., 2018. Asymmetric covalent triazine framework for enhanced visible-light photoredox catalysis via energy transfer cascade. *Angewandte Chemie International Edition*, 57(27):8316-8320. https://doi.org/10.1002/anie.201801112

Huang W, He Q, Hu YP, et al., 2019. Molecular heterostructures of covalent triazine frameworks for enhanced photocatalytic hydrogen production. *Angewandte Chemie*, 131(26):8768-8772. https://doi.org/10.1002/ange.201900046

Kong Z, Lu L, Zhu C, et al., 2022. Enhanced adsorption and photocatalytic removal of PFOA from water by F-functionalized MOF with in-situ-growth TiO_2: regulation of electron density and bandgap. *Separation and Purification Technology*, 297:121449. https://doi.org/10.1016/j.seppur.2022.121449

Li JH, Shen B, Hong ZH, et al., 2012. A facile approach to synthesize novel oxygen-doped g-C_3N_4 with superior visible-light photoreactivity. *Chemical Communications*, 48(98):12017-12019. https://doi.org/10.1039/C2CC35862J

Li LY, Fang W, Zhang P, et al., 2016. Sulfur-doped covalent triazine-based frameworks for enhanced photocatalytic hydrogen evolution from water under visible light. *Journal of Materials Chemistry A*, 4(32):12402-12406. https://doi.org/10.1039/C6TA04711D

Lu F, Astruc D, 2020. Nanocatalysts and other nanomaterials for water remediation from organic pollutants. *Coordination Chemistry Reviews*, 408:213180. https://doi.org/10.1016/j.ccr.2020.213180

Niu Q, Cheng Z, Chen QS, et al., 2021. Constructing nitrogen self-doped covalent triazine-based frameworks for visible-light-driven photocatalytic conversion of CO_2 into CH_4. *ACS Sustainable Chemistry & Engineering*, 9(3):1333-1340. https://doi.org/10.1021/acssuschemeng.0c07930

Qian ZF, Wang ZJ, Zhang KAI, 2021. Covalent triazine frameworks as emerging heterogeneous photocatalysts. *Chemistry of Materials*, 33(6):1909-1926. https://doi.org/10.1021/acs.chemmater.0c04348

Ren SJ, Bojdys MJ, Dawson R, et al., 2012. Porous, fluorescent, covalent triazine-based frameworks via room-temperature and microwave-assisted synthesis. *Advanced Materials*, 24(17):2357-2361. https://doi.org/10.1002/adma.201200751

Sarkar P, Chowdhury AH, Biswas S, et al., 2021. 2D covalent organic framework: a photoactive heterogeneous catalyst for chemical fixation of CO_2 over propargyl amines in water under sunlight. *Materials Today Chemistry*, 21:100509. https://doi.org/10.1016/j.mtchem.2021.100509

Shen Y, Zhu C, Song S, et al., 2019. Defect-abundant covalent triazine frameworks as sunlight-driven self-cleaning adsorbents for volatile aromatic pollutants in water. *Environmental Science & Technology*, 53(15):9091-9101. https://doi.org/10.1021/acs.est.9b02222

Ventosa E, Mei B, Xia W, et al., 2013. TiO_2(B)/anatase composites synthesized by spray drying as high performance negative electrode material in Li-ion batteries. *ChemSusChem*, 6(8):1312-1315. https://doi.org/10.1002/cssc.201300439

Vickers NJ, 2017. Animal communication: when I'm calling you, will you answer too? *Current Biology*, 27(14):R713-R715. https://doi.org/10.1016/j.cub.2017.05.064

Wang CC, Guo Y, Yang Y, et al., 2014. Sulfur-doped polyimide photocatalyst with enhanced photocatalytic activity under visible light irradiation. *ACS Applied Materials & Interfaces*, 6(6):4321-4328. https://doi.org/10.1021/am500007u

Xu JJ, Zhu C, Song S, et al., 2022. A nanocubicle-like 3D adsorbent fabricated by in situ growth of 2D heterostructures for removal of aromatic contaminants in water. *Journal of Hazardous Materials*, 423:127004. https://doi.org/10.1016/j.jhazmat.2021.127004

Xu JJ, Lu L, Zhu C, et al., 2023. Insights into conduction band flexibility induced by spin polarization in titanium-based metal-organic frameworks for photocatalytic water splitting and pollutants degradation. *Journal of Colloid and Interface Science*, 630:430-442. https://doi.org/10.1016/j.jcis.2022.10.015

Zhang YM, Hu YM, Zhao JH, et al., 2019. Covalent organic framework-supported Fe-TiO_2 nanoparticles as ambient-light-active photocatalysts. *Journal of Materials Chemistry A*, 7(27):16364-16371. https://doi.org/10.1039/C9TA03649K

Zhu BC, Zhang LY, Cheng B, et al., 2018. First-principle calculation study of tri-*s*-triazine-based g-C_3N_4: a review. *Applied Catalysis B: Environmental*, 224:983-999. https://doi.org/10.1016/j.apcatb.2017.11.025

Zhu C, Shen Y, Wang SB, et al., 2021a. Bidirectional progressive optimization of carbon and nitrogen defects in solar-driven regenerable adsorbent to remove UV-filters from water. *ACS ES&T Engineering*, 1(3):456-466. https://doi.org/10.1021/acsestengg.0c00176

Zhu C, Song S, Fang QL, et al., 2021b. Optimized pore configuration in solar-driven regenerable adsorbent for organic micro-pollutants removal. *Chemical Engineering Journal*, 426:131244. https://doi.org/10.1016/j.cej.2021.131244

Zhu C, Fang QL, Liu RL, et al., 2022. Insights into the crucial role of electron and spin structures in heteroatom-doped covalent triazine frameworks for removing organic micropollutants. *Environmental Science & Technology*, 56(10):6699-6709. https://doi.org/10.1021/acs.est.2c01781

Zhu C, Lu L, Xu JJ, et al., 2023. Metal monovacancy-induced spin polarization for simultaneous energy recovery and wastewater purification. *Chemical Engineering Journal*, 451:138537. https://doi.org/10.1016/j.cej.2022.138537

Zhu YK, Zhang Y, Cheng LL, et al., 2020. Novel application of g-C_3N_4/$NaNbO_3$ composite for photocatalytic selective oxidation of biomass-derived HMF to FFCA under visible light irradiation. *Advanced Powder Technology*, 31(3): 1148-1159. https://doi.org/10.1016/j.apt.2019.12.040

Electronic supplementary materials

Sections S1–S3, Table S1, Figs. S1–S4